ChemComm

COMMUNICATION

View Article Online
View Journal

Check for updates

Cite this: DOI: 10.1039/d5cc02952j

Received 24th May 2025,
Accepted 25th July 2025

DOI: 10.1039/d5cc02952j

rsc.li/chemcomm

Published on 01 August 2025. Downloaded by Yunnan University on 8/24/2025 8:54:32 PM.

From micro-to-nano in charged water microdroplets: unveiling steps in the weathering of minerals†

Anubhav Mahapatra,[a] Anirban Som,[a] B. K. Spoorthi,[a] Depanjan Sarkar[ac] and Thalappil Pradeep *[abc]

The recent discovery of the rapid conversion of micron-sized common minerals to nanoparticles in charged water microdroplets has attracted significant attention. Here, we studied this micro-to-nano transition as a function of applied electric potential and tip-to-substrate distance using high-resolution transmission electron microscopy (HRTEM). Our observations revealed that the fragmentation progresses through distinct stages, from larger particles to flower-like intermediates and finally to nanoparticles. The results suggested the need for a critical droplet size to initiate the disintegration process, with Coulomb explosion playing a significant role in particle scission. Our results provide new insights for the efficient green synthesis of nanomaterials.

Nanoparticles of common minerals have garnered significant attention from the scientific community due to their distinct physicochemical properties compared to their bulk counterparts. These attributes have driven their applications in agriculture, where engineered nanoparticles (*e.g.*, ZnO, SiO_2) enhance soil fertility and crop yield.[1,2] However, conventional nanoparticle synthesis methods often involve harsh chemicals and extreme conditions, raising sustainability concerns. These processes generate harmful byproducts, consume excessive energy, and limit scalability – key barriers for the development of green nanotechnology.[3]

Charged water microdroplets have emerged as a sustainable alternative for accelerating chemical reactions, acting as highly efficient microreactors that can speed up processes by orders of magnitude. Water is the most sustainable reaction medium. While water droplets have long been considered important in various environmental contexts,[4] their unique properties and reactivity have captured significant scientific attention only recently. In the laboratory, these microdroplets can be generated using electrospray, which stands out among related techniques for its ability to produce charged droplets with extreme interfacial electric fields (up to $\sim 10^9$ V m^{-1}). These intense fields promote the separation of hydronium and hydroxide ions, concentrate reactants at the droplet air–water interface,[5,6] and accelerate solvent evaporation, creating a dynamic environment that dramatically enhances reaction rates and enables the rapid formation of functional nanomaterials. Beyond accelerating organic reactions,[7,8] this can cause unusual phenomena to happen, like chemical reactions in the surrounding gas induced by luminescence.[9] Apart from this, charged microdroplets have also shown immense promise in fabricating a variety of nanomaterials.[10] Our research group has demonstrated the creation of structures ranging from zero-dimensional nanoparticles to three-dimensional nanopyramids, as well as large-area microstructures, all under ambient conditions and directly from salt precursors without the need for any external reagents.[11,12] This approach not only streamlines synthesis, but also enhances sustainability. Notably, we found that, in addition to forming nanomaterials from dissolved ions, charged water microdroplets can even fragment hard mineral microparticles such as quartz, reducing them to nanoparticles—a surprising and powerful capability that further expands the potential of this technique.[13,14] Ever since this discovery, there has been growing interest in understanding the mechanism behind this rapid transformation. While studies have also reported the conversion of nanosheets to nanoparticles in similar conditions,[15] the field has moved beyond simply observing these conversions to probing the underlying process. This was supported by density functional theory (DFT) calculations. The presence of various reactive species such as $OH^{\bullet}$, $H_2O^{+\bullet}$, H_2O_2, and others in droplets was speculated in the literature.[6] One recent investigation at the interface of oil droplets using Raman spectroscopy has focused on elucidating the structure and orientation of water molecules and the results have shown that oil–water emulsion interfaces exhibit reduced water structural order

[a] DST Unit of Nanoscience (DST UNS) & Thematic Unit of Excellence (TUE), Department of Chemistry, Indian Institute of Technology Madras (IITM), Chennai 600036, India. E-mail: pradeep@iitm.ac.in
[b] International Centre for Clean Water, 2nd Floor, B-Block, IIT Madras Research Park, Kanagam Road, Taramani, Chennai 600113, India
[c] Centre of Excellence on Molecular Materials and Functions, Department of Chemistry, Indian Institute of Technology Madras, Chennai – 600036, India

† Dedicated to Prof. Robert Graham Cooks on his 84th birthday.

Published on 01 August 2025. Downloaded by Yunnan University on 8/24/2025 8:54:32 PM.

and weaker hydrogen bonding. This is evidenced by a ~95 cm^{-1} redshift of the free O–H stretch compared to planar interfaces.[16] The involvement of protons in the process leading to silicate species among the fragmented products was confirmed by mass spectrometric measurements. From all of these, a tentative mechanism was drawn, but a key question remained as to whether the mineral underwent fragmentation within the water droplet itself and got deposited on the substrate as nanoparticles. In the present work, we demonstrate a systematic investigation of the fragmentation process; we observed distinct stages in the disintegration of micron-sized mineral particles within charged microdroplets. Notably, during the intermediate stage of fragmentation, we captured unique flower-like structures, providing visual evidence of the ongoing breakdown. These intermediate forms were crucial in demonstrating that mineral fragmentation occurs within the droplets during their flight, rather than after deposition. Our findings also confirm that the applied electrical potential is the most fundamental and decisive factor influencing the outcome of the process. The experiment involved generating charged water microdroplets using electrospray, as described previously and detailed in the SI, with an important modification. Specifically, we collected the deposited products at an applied potential of 3.5 kV and varying distances (L) from the electrospray tip, as shown in Fig. 1A and detailed in Fig. S1, SI, while maintaining all other experimental conditions constant. For these experiments, quartz particles (5–10 μm) were suspended in ultrahigh-purity water (18 MΩ Milli-Q) at a concentration of 0.2 mg mL^{-1} and electrosprayed at a flow rate of approximately 0.1 mL $hour^{-1}$. The suspension was subjected to electrospray at varied collection distances to capture different stages of particle fragmentation. Optical images of the bulk micron-sized quartz powder and high-resolution SEM images are shown in Fig. 1B and 1C, respectively. The electrospray was directed onto a TEM grid for product collection and subsequent imaging. By collecting samples at various tip-to-substrate distances, specifically at 1.5, 2.0, and 2.5 cm, as schematically demonstrated in Fig. 1A, we observed significant variation in the fate of the micron-sized particles. At the shortest distance (1.5 cm), TEM images (Fig. 1D) revealed that the particles largely remained intact as larger aggregates. As the distance increased to 2.0 cm, partial fragmentation was observed, with distinctive flower-like intermediate structures captured in the TEM images (Fig. 1E). When the distance was further increased to 2.5 cm, complete fragmentation occurred, resulting in monodisperse nanoparticles as shown in Fig. 1F.

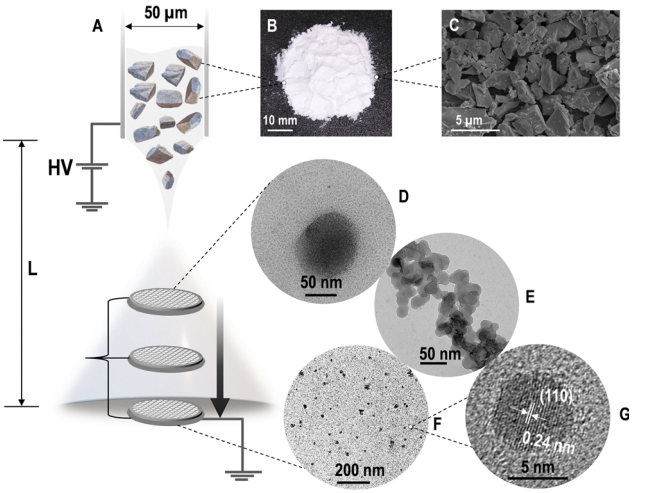

Fig. 1 The disintegration process of natural quartz particles in charged water microdroplets. Schematic diagram showing the different components of the home-built electrospray set-up with (A) a fused silica capillary of inner diameter 50 μm, (B) an optical image of the ground quartz powder, and (C) field emission scanning electron microscopy (FESEM) of the separated quartz particles revealing the size range of 5 to 10 μm. Transmission electron microscopic (TEM) images of these particles after electrospray deposition at an applied potential of 3.5 kV, with varying tip-to-substrate distances of (D) 1.5 cm, (E) 2.0 cm, and (F) 2.5 cm, demonstrating different stages of fragmentation. (G) High-resolution TEM (HRTEM) image showing the (110) plane of quartz.

All these experiments described here were performed under identical conditions except varying the tip-to-substrate distance. As evident from the data, the flight time of the microdroplets has a great impact on the weathering process. High-resolution TEM (HRTEM) images, presented in Fig. 1G and Fig. S2, SI, confirmed the identity of these nanoparticles as quartz, based on the lattice spacing of 0.24 nm, which corresponds to the (110) plane of quartz.

A detailed study was performed in which aqueous suspensions of quartz (0.2 mg mL^{-1}) were electrosprayed, and the resultant charged microdroplets were collected at varying tip-to-substrate distances under fixed applied potentials. This experiment was repeated across a range of potentials (3.0–4.5 kV). A systematic series of TEM images is summarized in Fig. 2. At 3 kV, no particle disintegration was observed as reported previously. At 3 kV, at a tip-to-substrate distance of 1.5 cm, the particles remained largely intact. However, at 2.0 cm, flower-like intermediate structures were captured in the TEM images, indicating ongoing fragmentation, while complete disintegration into nanoparticles was achieved at 2.5 cm. A similar trend was observed at 3.5 kV. When the potential was increased to 4 kV, fragmentation was initiated even at the shorter distance of 1.5 cm, and monodisperse nanoparticles were formed at 2.0 and 2.5 cm. At 4.5 kV, complete disintegration was observed at 1.5 cm, demonstrating that higher potentials and longer distances facilitate efficient fragmentation. A distinct boundary (marked by a red dotted line in Fig. 2) was established to delineate the threshold for effective disintegration, emphasizing the critical role of smaller, highly charged droplets in particle scission. At lower potentials and shorter distances, flower-like intermediates were identified, suggesting a stepwise cleavage process within the micron-sized particles, during flight. The control experiments with neutral droplets are detailed in Fig. S5 and section S4, SI to rule out other factors dominating fragmentation.

A similar set of observations was made when ruby (0.2 mg mL^{-1}) was subjected to the same electrospray conditions, with all other experimental parameters kept constant, and the results are presented in Fig. 3. FESEM images of ruby before electrospray are

 This journal is © The Royal Society of Chemistry 2025

Published on 01 August 2025. Downloaded by Yunnan University on 8/24/2025 8:54:32 PM.

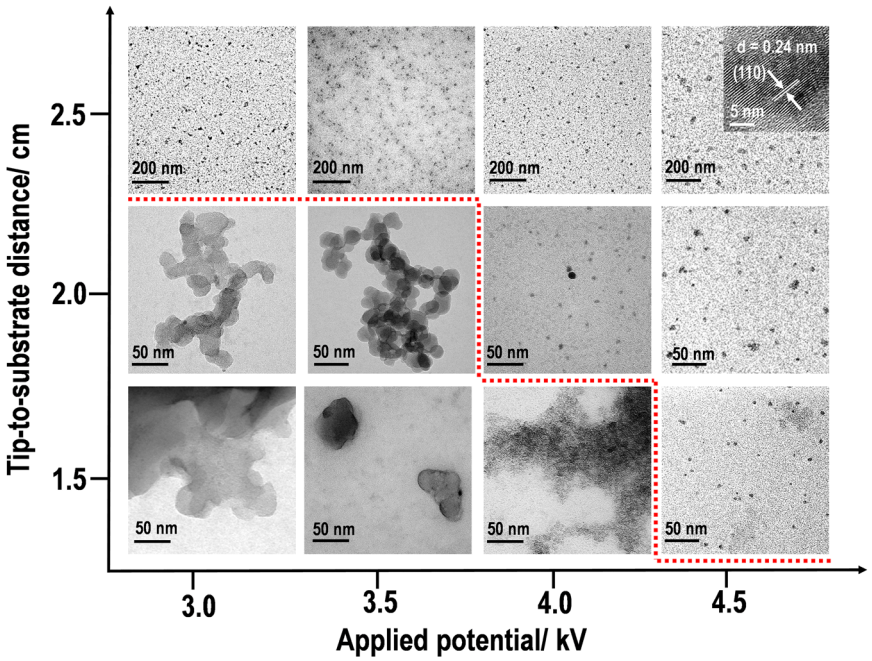

Fig. 2 TEM images showing the disintegration pathway of quartz particles as a function of applied potential (in kV) and tip-to-substrate distance (in cm). The applied potential was varied from 3 to 4.5 kV and tip-to-substrate distance was varied from 1.5 to 2.5 cm. The potential and distance values for an experiment are indicated at the centre of the corresponding TEM images. The dotted line differentiates the relatively big particles of quartz from the nanoparticles. An HRTEM image of one particle showing the (110) plane of quartz is placed as an inset.

shown in Fig. S3, SI. At a lower potential of 3 kV, fragmentation of ruby particles was observed only at a tip-to-substrate distance of 2.5 cm. When the potential was increased to 4.0 kV, flower-like intermediate structures were captured at 2.0 cm, and complete disintegration into nanoparticles was achieved at 2.5 cm. However, even at 5 kV, fragmentation was not complete at shorter distances, indicating that ruby requires higher potential due to its greater hardness and mechanical strength for the complete disintegration of ruby compared to quartz. This difference may be attributed to the higher elastic modulus and Mohs hardness of ruby ($\geq$9) relative to quartz ($\geq$7).[17] A detailed explanation is provided in S5, SI. The effect is particularly evident at a distance of 1.5 cm and potential of 5 kV, where ruby particles remain larger and do not fully fragment, in contrast to the behaviour observed for quartz. Nanoparticle formation was observed at 2.5 cm under all tested conditions, underscoring the importance of smaller droplets with a higher surface-to-volume ratio in facilitating the process. From the TEM images, it can be speculated that ruby exhibits more gradual fragmentation than quartz, which may be attributed to its higher hardness. HRTEM images, presented in Fig. 3 and Fig. S4, SI, reveal a lattice spacing of 0.23 nm, corresponding to the (110) plane of ruby. The size distribution of the nanoparticles along with the EDS analysis of flower-like intermediate species of quartz and ruby are shown in Fig. S6–S8, SI.

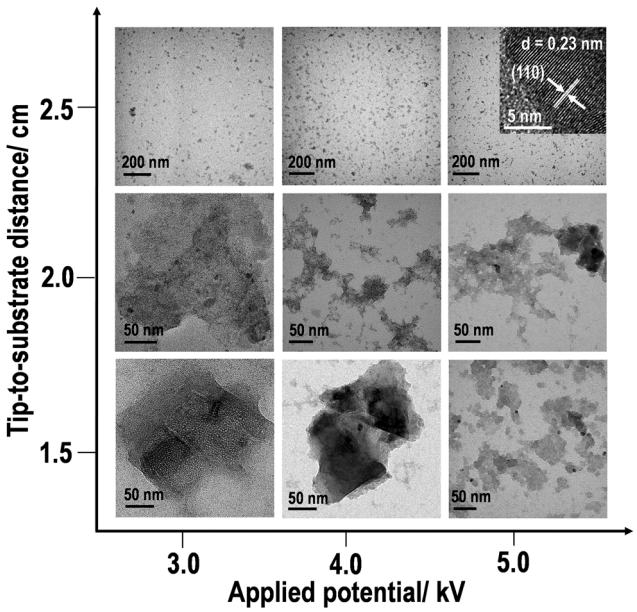

Fig. 3 TEM images showing the disintegration pathway of ruby particles into nanoparticles as a function of applied potential (in kV) and tip-to-substrate distance (in cm). The applied potential varies from 3 to 5.0 kV and the tip-to-substrate distance varies from 1.5 to 2.5 cm. The indicated potential and distance values are placed at the centre of the TEM images. An HRTEM image of one particle showing the (110) plane of ruby is placed as an inset.

To further investigate the dependence of mineral disintegration on the electric field, an experiment was conducted using quartz particles while maintaining a constant electric field strength of E = 3 kV cm^{-1}. This was achieved by keeping the ratio of applied potential to tip-to-substrate distance constant across all trials. The results, presented in Fig. 4, show that while the electric field was held steady, the applied potential along with tip-to-substrate distance are clearly the critical parameters influencing the fragmentation process.

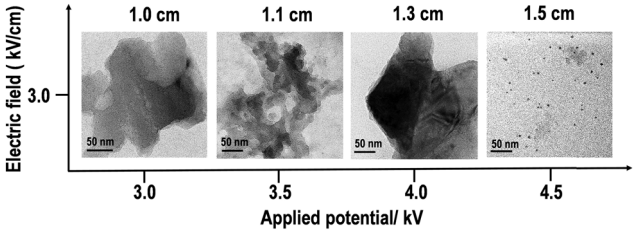

Fig. 4 TEM images showing the particle size of quartz collected at varied conditions of potential and tip-to-substrate distance to maintain the constant electric field of 3 kV cm^{-1}.

It was observed that a minimum tip-to-substrate distance of 1.5 cm was necessary for the disintegration of quartz to occur within the charged water microdroplets. These findings emphasize that, although both electric field strength and distance are important, the absolute value of the applied potential plays a decisive role in enabling mineral fragmentation under these conditions. Collectively, these results indicate that mineral disintegration within charged water microdroplets is strongly influenced by both applied potential and droplet dynamics. At high potentials and optimal tip-to-substrate distances, charged droplets will reach the Rayleigh limit, leading to Coulomb explosion of the droplets along with particle fragmentation. Alternatively, or in parallel, the buildup of intense electric fields during the Coulomb explosion can generate highly charged regions that, in turn, facilitate the formation of reactive species (*e.g.*, hydroxyl radicals or protons) which can induce mineral fragmentation. Both pathways may contribute to the observed disintegration process. Incomplete disintegration at lower potentials or shorter distances suggests that a threshold in droplet size and charge must be surpassed for nanoparticle formation. Overall, the findings suggest that electrical, mechanical and chemical effects within the shrinking charged droplets are important for efficient mineral fragmentation and nanoparticle synthesis.

In conclusion, we established that the key factor in determining particle scission in charged water microdroplets is the applied potential and flight distance. Disintegration occurs within the droplets. This outcome establishes the significance of a critical size for a droplet in inducing disintegration. This can be a way forward in deciding the optimal parameters to synthesize nanoparticles of any material in charged water microdroplets. Observing flower-like intermediates within the droplets at the critical size will be important in establishing the finer details of the events involved. In future, detailed computational and statistical studies will be needed to assess the degree of fragmentation and its underlying mechanism.

The authors thank the Anusandhan National Research Foundation (ANRF), Department of Science and Technology (DST), University Grant Commission (UGC), Government of India and Centre of Excellence on Molecular Materials and Functions under the Institution of Eminence Scheme of IIT Madras for generous funding and supporting our research on nanomaterials. TEM measurements were collected at the ANRF National Facility for Cryo-Electron Microscopy at IIT Madras.

Conflicts of interest

There are no conflicts to declare.

Data availability

The data supporting this article are included in the main article and its SI. No additional data have been deposited in external repositories.

Supplementary information is available. See DOI: **https://doi.org/10.1039/d5cc02952j**.

Notes and references

1 L. V. Subbaiah, T. N. V. K. V. Prasad, T. G. Krishna, P. Sudhakar, B. R. Reddy and T. Pradeep, *J. Agric. Food Chem.*, 2016, **64**, 3778–3788.
2 Z. Kang, J. Lu, S. Zheng, X. Hu, L. Wang, L. Jiang, Y. Zheng, L. Lv, J. L. Gardea-Torresdey, J. C. White and L. Zhao, *ACS Nano*, 2025, **19**, 3752–3763.
3 D. G. Gomes, J. C. Pieretti, C. N. Lange, B. D. M. Santana, B. L. Batista, P. S. Parreira, C. Zucareli, A. B. Seabra and H. C. Oliveira, *ACS Appl. Nano Mater.*, 2024, **7**, 20058–20070.
4 X. Jia, J. Wu and F. Wang, *JACS Au*, 2024, **4**, 4141–4147.
5 H. Wei, E. P. Vejerano, W. Leng, Q. Huang, M. R. Willner, L. C. Marr and P. J. Vikesland, *Proc. Natl. Acad. Sci. U. S. A.*, 2018, **115**, 7272–7277.
6 J. Zhou, Q. Wang, G. Cheng, W. Shen, R. N. Zare and X. Sun, *J. Am. Chem. Soc.*, 2025, **147**, 10916–10924.
7 Y. Wu, J. Li, J. Sun, Y. Wang, J. Liu and H. Cheng, *J. Org. Chem.*, 2024, **89**, 18493–18503.
8 K. Naveen, V. S. Rawat, R. Verma and E. Gnanamani, *Chem. Commun.*, 2024, **60**, 13263–13266.
9 Y. Meng, Y. Xia, J. Xu and R. N. Zare, *Sci. Adv.*, 2025, **11**, eadt8979.
10 Z. Wei, Y. Li, R. G. Cooks and X. Yan, *Annu. Rev. Phys. Chem.*, 2020, **71**, 31–51.
11 A. Jana, S. K. Jana, D. Sarkar, T. Ahuja, P. Basuri, B. Mondal, S. Bose, J. Ghosh and T. Pradeep, *J. Mater. Chem. A*, 2019, **7**, 6387–6394.
12 D. Sarkar, M. K. Mahitha, A. Som, A. Li, M. Wleklinski, R. G. Cooks and T. Pradeep, *Adv. Mater.*, 2016, **28**, 2223–2228.
13 B. K. Spoorthi, K. Debnath, P. Basuri, A. Nagar, U. V. Waghmare and T. Pradeep, *Science*, 2024, **384**, 1012–1017.
14 R. G. Cooks and D. T. Holden, *Science*, 2024, **384**, 958–959.
15 B. K. Spoorthi, A. R. Chowdhuri, B. Mondal, S. Manna, A. Mahapatra, A. R. Kini and T. Pradeep, *Chem. Commun.*, 2025, **61**, 5577–5580.
16 L. Shi, R. A. LaCour, N. Qian, J. P. Heindel, X. Lang, R. Zhao, T. Head-Gordon and W. Min, *Nature*, 2025, **640**, 87–93.
17 S. Ruppi, A. Larsson and A. Flink, *Thin Solid Films*, 2008, **516**, 5959–5966.

Published on 01 August 2025. Downloaded by Yunnan University on 8/24/2025 8:54:32 PM.

 This journal is © The Royal Society of Chemistry 2025